

A universal stellar-mass and size relation of galaxies in GOODS-N region

Takashi Ichikawa,^{1*} Masaru Kajisawa,² and Mohammad Akhlaghi¹

¹*Astronomical Institute, Tohoku University, Aramaki, Aoba, Sendai 980-8578, Japan*

²*Research Center for Space and Cosmic Evolution, Ehime University, Bunkyo-cho 2-5, Matsuyama 790-8577, Japan*

Accepted. Received; in original form

ABSTRACT

We present scaling relations between stellar-mass (M_*) and the size of galaxies at $0.3 < z < 3$ for half- (R_{50}) and 90 percent-light (R_{90}) radii, using a deep K -band selected catalogue taken with the Subaru Telescope and MOIRCS in the GOODS-North region. The logarithmic slope $R \propto M_*^{0.1 \sim 0.2}$ is independent of redshift in a wide mass range of $M_* \sim 10^8 - 10^{11} M_\odot$, irrespective of galaxy populations (star-forming, quiescent). The offset change is $\lesssim 50$ percent. Provided that optical light in the rest frame traces the stellar mass of galaxies, the universal relation demonstrates that the stellar mass was built up in galaxies over their cosmic histories in a similar manner on average irrelevant to galaxy mass. The small offset in each stellar mass bin from the universal relation shows weak size evolution at a given mass. There is a moderate increase of 30–50 percent for R_{50} and R_{90} for less massive galaxies ($M_* < 10^{10} M_\odot$) from $z \sim 3$ to $z \sim 1$, while the sizes remains unchanged or slightly decrease towards $z \sim 0.3$. For massive galaxies ($M_* \gtrsim 10^{11} M_\odot$), the evolution is $\sim 70 - 80$ % increase in R_{90} from $z \sim 3$ to $z \sim 0.3$, though that in R_{50} is weaker. The evolution of compactness factor, R_{50}/R_{90} , which becomes smaller at lower redshift, is suggestive of minor merging effect in the outer envelope of massive galaxies.

Key words: galaxies: evolution – galaxies: fundamental parameters – galaxies: high-redshift – infrared: galaxies.

1 INTRODUCTION

The scale size of galaxies is one of the fundamental parameters to elucidate the history of galaxy formation and evolution. The change of size and stellar-mass relations over cosmic time would pose strong constraints on models of galaxy evolution. The observational relations between galaxy size and stellar mass have been studied in the local universe, based on the Sloan Digital Sky Survey (Shen et al. 2003; Bernardi et al. 2011). Using rest-frame optical bands, which presumably trace the distribution of stellar mass in galaxies, many studies have investigated galaxy sizes at higher redshift as a function of stellar mass for massive galaxies ($M_* \gtrsim 10^{10} M_\odot$). For example, the relations for galaxies at $0.2 < z < 1$ were studied for late-type galaxies (Barden et al. 2005) and for early-type galaxies (McIntosh et al. 2005; Trujillo, Ferreras, & de la Rosa 2011). Damjanov et al. (2009) and Mancini et al. (2010) gave size-mass relations of massive galaxies ($M_* > 10^{10.5} M_\odot$) at $z \sim 1.5$. Williams et al. (2010) studied the relation with large samples of galaxies at $z \lesssim 2$. For higher redshifts to $z \sim 3$, size-mass relations have been obtained for galaxies with $M_* \gtrsim 10^{10} M_\odot$ (e.g., Franx et al. 2008; Nagy et al. 2011; Cassata et al. 2011).

Many studies have corroborated that massive galaxies at high

redshifts were much smaller than local galaxies with comparable mass (e.g., Daddi et al. 2005; Trujillo et al. 2006, 2007; Toft et al. 2007; Zirm et al. 2007; Cimatti et al. 2008; Buitrago et al. 2008; van Dokkum et al. 2008, 2009, 2010; Akiyama et al. 2008; Damjanov et al. 2009; Carrasco et al. 2010; Cassata et al. 2010; Szomoru et al. 2010; van der Wel 2011; Cassata et al. 2011). At a fixed stellar mass, spheroidal galaxies were significantly more compact at high redshift and evolved with rapid increase of the effective radius by a factor ~ 4 or even larger from $z \sim 2$ (e.g., Buitrago et al. 2008; Carrasco et al. 2010) and by a factor ~ 2 from $z \sim 1$ (e.g., van der Wel et al. 2008; Trujillo et al. 2011). The finding of compact massive galaxies with a high stellar velocity dispersion also supports their existence (van Dokkum 2009; van de Sande 2011). It contrasts with the absence of such compact massive galaxies in the local universe, though several candidates have been found at $z \sim 0.5$ (Stockton et al. 2010) and in the local universe (Trujillo et al. 2009; Valentini et al. 2010). The findings demonstrate that massive galaxies have increased their size dramatically since $z \sim 3$ in a different manner from the evolution of less massive galaxies.

However, other studies have reached contradictory conclusions. There is significant disagreement between the results of different studies. Barden et al. (2005) found weak or no evolution in the relation between stellar mass and effective disc size for galaxies with $M_* > 10^{10} M_\odot$ since $z \sim 1$. For early-type galaxies at

* E-mail: ichikawa@astr.tohoku.ac.jp

$z \sim 1$, McIntosh et al. (2005) showed that luminosity-size and stellar mass size relations evolve in a manner that is consistent with a completely passive evolution of the red early-type galaxy population. It is also shown that not all high-redshift early-type galaxies were compact and underwent dramatic size evolution (e.g., Toft et al. 2007; Zirm et al. 2007; Saracco et al. 2009, 2011; Mancini et al. 2010; Stott et al. 2011). From the study of surface brightness in rest-frame V and z bands at $z \lesssim 3$, Ichikawa et al. (2010) gave another evidence for no conspicuous evolution in galaxy sizes.

As many previous studies show, the size evolution of galaxies are still controversial. Any systematic errors in the observation or analyses could bias results towards such a significant evolution (e.g., Mancini et al. 2010; Hopkins et al. 2009b; Bouwens et al. 2004). The origin of the discrepancy could be ascribed to redshift effects that more distant galaxies look more compact due to the difficulty of measuring envelopes at low surface density. The light from the outer portion of high-redshift galaxies is apt to be hidden in noise for low S/N observations. As the consequence, effective radii and total luminosity (or stellar mass) would be underestimated. On the other hand, very deep observations (e.g., Szomoru et al. 2010; Cassata et al. 2010; Law et al. 2012) or stacking methods to enhance the faint envelope of galaxies (e.g., Zirm et al. 2007; van Dokkum et al. 2008, 2010; van der Wel et al. 2008) have claimed that it is not the case.

How significantly have the sizes of less-massive normal galaxies evolved from the early universe to the current epoch? In this context, we look into the evolution of stellar-mass and size scaling relations on the basis of half- and 90 percent-light encircles, focusing on less massive galaxies ($M_* < 10^{11} M_\odot$) at $0.3 < z < 3$, using a deep K -selected galaxy catalogue. We infer that the outer radius is more influenced by merging effect than star formation or central activity. In §2, we describe the catalogue we used, which is among the deepest in the K band to date. The depth is crucial for studying galaxies of low-surface brightness or galaxies which are dimmed due to the cosmological expansion at high redshift to measure the radius at faint outskirts of galaxies. The data analysis and the result for the size and stellar-mass relation are detailed in §3 and §4. The results are discussed in §5. Ichikawa et al. (2010) studied the evolution of surface brightness of galaxies at $z \lesssim 3$ in rest-frame V and z bands with the same data as the present study. We will discuss the consistency of the present result with their study.

Throughout this paper, we assume $\Omega_m = 0.3$, $\Omega_\Lambda = 0.7$, and $H_0 = 70 \text{ km s}^{-1} \text{ Mpc}^{-1}$. We use the AB magnitude system (Oke & Gunn 1983; Fukugita et al. 1996).

2 DATA

We use the K -band selected catalogue of the MOIRCS Deep Survey (MODS) in the GOODS–North region (Kajisawa et al. 2009, hereafter K09; Kajisawa et al. 2011, K11), which are based on our imaging observations in $JHKs$ bands with MOIRCS (Suzuki et al. 2008) and archived data. Four MOIRCS pointings cover 70 percent of the GOODS–North region (103 arcmin^2 , hereafter referred as ‘wide’ field). One of the four pointings, which includes HDF-N (Williams et al. 1996), is the ultra-deep field of MODS (28 arcmin^2 , ‘deep’ field). As the accuracy of background subtraction was highly demanded for the study of faint end of galaxies, the background was scrutinized and carefully subtracted (see K11 for the details). The surface brightness limit was extensively examined in K11. The typical 1σ surface brightness fluctuations in one arcsec diameter were found to be $\sim 27 \text{ mag arcsec}^{-2}$ and $\sim 27.5 \text{ mag arcsec}^{-2}$ in

K band for the wide and deep fields respectively. These are $1 \sim 2$ mag deeper than those of previous studies in K band. The depth is crucial for the study of low surface brightness features at the outskirts of galaxies because of the strong dependence of cosmological dimming of surface brightness on redshift.

For the total magnitude m_K in K band, we use MAG_AUTO obtained by SExtractor (Bertin & Arnouts 1996). The 85 \sim 90-percent completeness of the catalogue is $m_K \sim 25$ in the wide field and ~ 26 mag in the deep field. We exclude fainter galaxies from the present analysis. The FWHMs of the final stacked images are 0.46 arcsec for the deep image and 0.53–0.60 arcsec for the wide image. The numbers of galaxies are 3555 and 6063, respectively.

To obtain the stellar mass of MODS samples, K09 performed SED fitting of the multiband photometry ($UBVizJHK$, $3.6 \mu\text{m}$, $4.5 \mu\text{m}$, and $5.8 \mu\text{m}$) with population synthesis models. We adopt the results with GALAXEV templates (Bruzual & Charlot 2003) and the Salpeter initial mass function (see K09 for more details). The stellar masses (M_*) are obtained from the best-fit stellar mass-to-luminosity ratio in K band and scaled with the K -band flux. A detailed comparison between different mass estimators is given in K09. In the present analysis, the near-infrared data ($3.6 \mu\text{m}$) of Spitzer/IRAC are available for most of the sample galaxies (96 percent), so that SED fitting is reasonably reliable for the photometry at rest- V ($\lambda_{\text{eff}} = 0.55 \mu\text{m}$) out to redshift ~ 3 . We assume that the size of the stellar system in galaxies is represented by the size measured on K -band images, which are the rest-frame optical to near-infrared wavelengths at $z \lesssim 3$. The difference of the sizes between optical and infrared light is discussed in §4.

In the present catalogue, 209 galaxies are identified as X-ray sources. Among them, 61 sources are massive galaxies emitting hard X-rays with $M_* > 10^{10.5} M_\odot$ at $2 < z < 4$ (Yamada et al. 2009). One would expect galaxies with AGN emission to have smaller half-light radius. Considering possible effects on the size and mass estimates, we discard X-ray sources in what follows.

3 ANALYSES

3.1 Galaxy sizes

As the definition of galaxy size, most previous studies have used the scale length (r_e), obtained by fitting the Sérsic profile (Sérsic 1968) to galaxy images. The accuracy of the scale length strongly depends on image quality and depth of observations. For bright galaxies, reliable galaxy sizes can be measured from ground-based data (Trujillo et al. 2006; Franx et al. 2008; Williams et al. 2010). On the other hand, it is crucial to take an accurate measure of the profile for small objects near the resolution limit. In fact, Konishi et al. (2011) applied two dimensional fitting for the present sample to obtain Sérsic indexes with a single component for a morphological study of MODS galaxies. However, they found that reliable fitting was successful only for comparatively massive galaxies ($M_* > 10^{10} M_\odot$) at $z \sim 1$ and very bright galaxies ($K < 22.5$) at higher redshift. The resolution of $\text{FWHM} = 0.5 \sim 0.6 \text{ arcsec}$ like the present sample would not allow reliable fitting with Sérsic profile to fainter galaxies. Sérsic parameters are sometimes degenerated between n and r_e , which depends on the surface-brightness limit of the images (e.g., Mancini et al. 2010; Stott et al. 2011), so that the reliable fitting would be difficult for faint galaxies. Moreover high-redshift galaxies exhibit a wide range of disturbed morphologies (e.g., Kajisawa & Yamada 2001). Therefore, the fitting for less massive galaxies at high redshift could also be strongly influenced

by their more amorphous features in the shape. In addition, we must take into account that we are observing a mix of galaxy morphologies.

As such, we define the half-light radius (r_{50}) as the radius of a circular aperture, which encircles half the K -band light emitted from galaxies. As we here focus not just on massive (or bright) galaxies, but also on less massive galaxies up to $z \sim 3$, we prefer r_{50} to r_e for the study of the structural parameters. If a galaxy profile extends to infinity, r_e encloses half the flux in the Sérsic profile. However, as galaxies are supposed to have an edge at several times the scale length, r_e does not always mean half-light radius. Therefore, in general, r_{50} is smaller than r_e . In the same way, we define 90 percent-light radius r_{90} . The 90-percent radius will give us more information at outer region of galaxies, where the size would be more influenced by merging effect. r_{50} and r_{90} are obtained by SExtractor with `PHOT_FLUXFRAC`=0.5 and 0.9

Figure 1 shows r_{50} versus m_K for all objects in MODS. MODS catalogue lists many spectroscopically confirmed stars, which are also plotted in Fig. 1. As few spectroscopic data were available for stars fainter than $m_K \sim 23.5$ in the present region, we examined the reliability of r_{50} using artificial stars. The artefacts were convolved with a Moffat point spread function ($\beta = 3$ and $\text{FWHM}=0.5$ arcsec in the deep field and 0.6 arcsec in the wide field), and then buried in images as noisy as those of the deep and wide fields. SExtractor was applied to the artefacts in the same manner as for the MODS catalogue. The results are plotted in Fig. 1. The location of stars gives a clear boundary of unresolved galaxies. We define galaxies smaller than $r_{50} = 0.41$ in the wide field $r_{50} = 0.30$ in the deep field as unresolved galaxies.

3.2 Monte Carlo study for the sizes with mock galaxies

We first study the reliability of the galaxy size. Seeing and background noise strongly affect the observed r_{50} and r_{90} , especially for faint or small galaxies. To examine the effect on the size estimate, we generated mock galaxies with a 1/4-law or exponential profile extending to 3 times scale length. The images are then convolved with a Moffat point spread function ($\beta = 3$ and $\text{FWHM}=0.5$ arcsec in the deep field and 0.6 arcsec in the wide field), and buried in the simulated noise image. The galaxies were randomly generated with various magnitudes and effective radii or scale lengths, and analyzed with SExtractor in the same manner as for the MODS galaxies. The results are shown in Fig. 2. Seeing and noise seriously change the observed radii specifically for galaxies with a 1/4-law profile. The observed r_{50} is significantly smaller than the intrinsic values in general. The effect is stronger for fainter 1/4-law galaxies, whereas the effect is much smaller for exponential galaxies. The apparent smaller size than the intrinsic size would be due to the fact that the faint and large envelope of 1/4-law galaxies is hidden in background noise. We should be aware of this effect if the observation is not deep enough for early-type galaxies (see also Hopkins et al. 2009b; Mancini et al. 2010). The effect will be discussed in more detail in the following section. It is noted that Williams et al. (2010) claimed no systematic effects on r_e for $m_K \lesssim 24$, using the shallower MODS images.

The radii, r_{50} and r_{90} , for small galaxies are affected by smearing due to seeing effect and the effect depends on galaxy morphology and size. Therefore, we obtained Eq. 1 to correct the size effect by fitting the deviation of the size as shown in Fig. 2 (dash line). However, it is hard to examine the shapes of the present small or high- z galaxies, so that we do not correct the effect which depends on morphology.

$$r_{\text{intrinsic}} = \sqrt{r_{\text{observed}}^2 - (\Delta r)^2}. \quad (1)$$

We adopt $\Delta r = 0.25$ and 0.35 arcsec for r_{50} and r_{90} , respectively.

The size errors for mock galaxies are depicted in Fig. 3 as a function of observed magnitude. We should take into account that much smaller values are obtained for the size of 1/4-law galaxies. Figure 4 is the difference between intrinsic and observed magnitudes. At the faint limit, observed magnitudes are fainter by $1 \sim 1.5$ mag for 1/4-law galaxies, while the effect is much smaller for exponential galaxies. These results suggest that shallower observations tend to more underestimate size and flux (therefore, stellar mass). We discuss later the influence on the results due to the systematic errors.

3.3 Size and stellar mass relations

Using photometric (or spectroscopic, if available) redshift data, r_{50} and r_{90} in arcsec are converted to the physical size in kpc (R_{50} and R_{90}). The photo- z accuracy of the present sample is reasonably good, $\delta z/(1+z) = -0.011$ ($\sigma = 0.078$) (K11), so that we expect no serious influence on our result due to the photo- z error. We will confirm this later using galaxies with spectroscopic redshifts. The results for R_{50} and R_{90} are shown in Figs. 5 and 6 as a function of the stellar mass of galaxies for different redshift bins. The unresolved galaxies are displayed in another figure (Fig. 7) for reference. The results of effective radius (r_e) for local galaxies by Shen et al. (2003) are also shown in Fig. 5 for comparison. Size-mass relations for star-forming galaxies are consistent with that of late-type galaxies by Shen et al. (2003), although our definition of half-light radius is different from that of Shen et al. (2003). It should be noted that it would be difficult to discuss the consistency for massive early-type galaxies because of the small number of such galaxies in our sample.

Since our image quality is not high enough for classifying the galaxies into morphological classes at high redshifts, we divided the samples into quiescent and star-forming galaxy groups using a two-color diagnostic plot of rest-frame $U - V$ and $V - J$ colors (Williams et al. 2009). The adopted selection criteria for quiescent galaxies are as follows:

$$(U - V) > 0.88(V - J) + c, \quad (2)$$

where $U - V$ and $V - J$ in the rest frame were obtained with the SED model fit to galaxies. The offset, c , is 0.69, 0.59, and 0.49 for $0.0 < z < 0.5$, $0.5 < z < 1.0$, and $1.0 < z < 2.5$, respectively. For $z > 2.5$ galaxies, we applied the offset for $1 < z < 2.5$. Therefore the selection would be less reliable (see Williams et al. 2009), though the number of such galaxies is very small. Additional criteria of $U - V > 1.3$ and $V - J < 1.6$ are required for quiescent galaxies at all redshifts to prevent contamination from unobscured and dusty star-forming galaxies, respectively.

3.4 Stellar-mass surface density

The small differences in the slope and offset of the regression lines in different redshift bins in Figs. 5 and 6 would imply a universal relation between the stellar mass and size of galaxies, irrelevant to redshift. In this context, we plot the stellar-mass surface density (SMSD), which is defined as $\mu_* = \log(M_*/\pi R^2)$, in a single redshift bin as a function of stellar mass for all galaxies at $0.25 < z < 3$ (Figs. 9 and 10). The figures are essentially equivalent to the size-mass distribution. However, we can easily identify

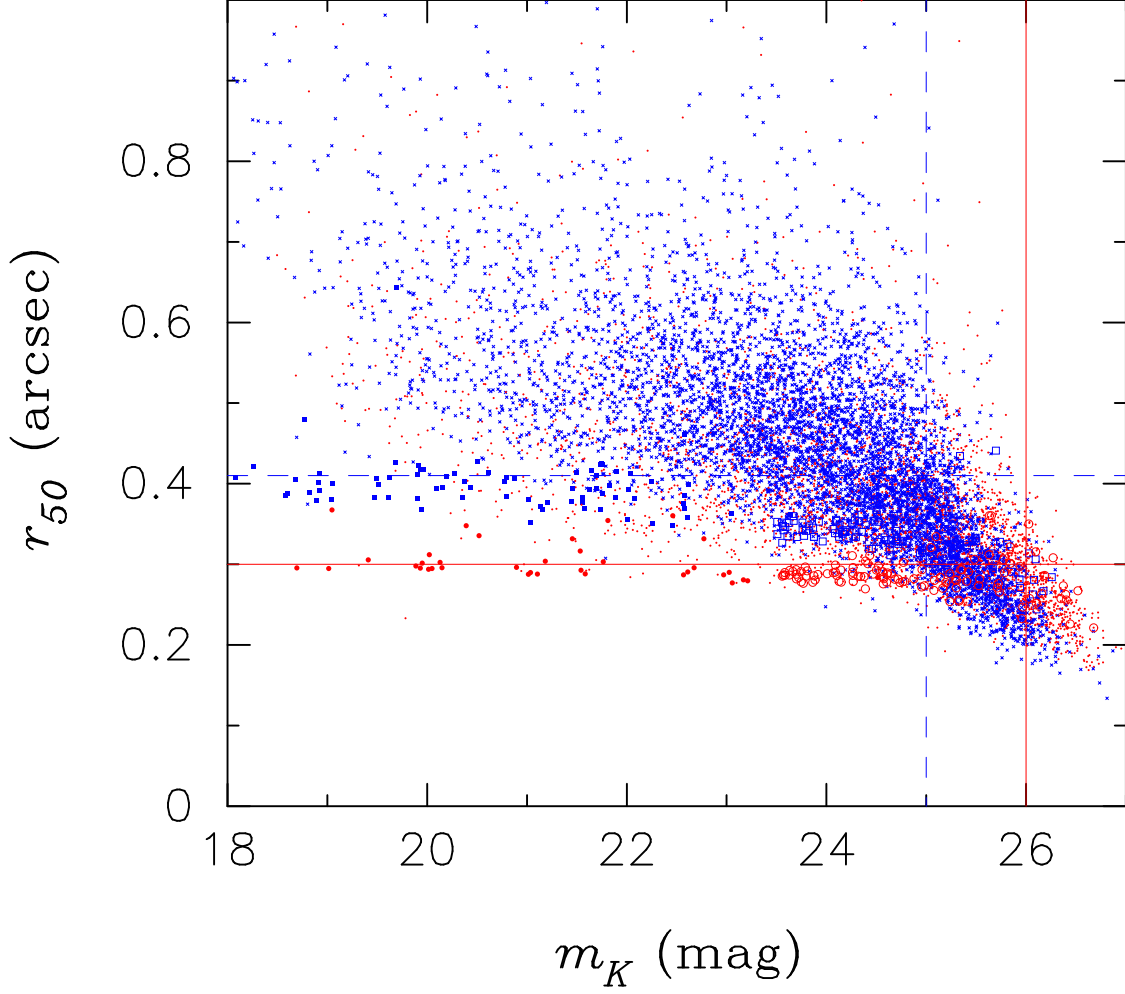


Figure 1. Half-light radius (r_{50}) and total magnitude (m_K) for the MODS catalogue. The dots (red) and crosses (blue) shows the samples in the deep and wide fields, respectively. The vertical solid and dashed lines indicate the magnitude limit for each field. Filled (blue) squares and circles (red) are spectroscopically confirmed stars. Few stars fainter than 23.5 mag with spectroscopic data are available, so that we plot the results of SExtractor detection of artificial stars embedded in noise images (open blue squares for the wide and open red circles for the deep). The horizontal (blue) dash and (red) solid lines delineates unresolved sources.

very compact or low-surface brightness galaxies in the figures, if they exist. For example, galaxies as compact (or diffuse) as 3 times smaller (larger) in size than the average should be located at ~ 1.0 dex above (below) the average. Such low surface brightness galaxies can be recognized at $M_* < 10^{10} M_\odot$ in Fig. 10.

In contrast, massive and compact galaxies are rare in the present sample. It is noted that most of massive galaxies with $M_* > 5 \times 10^{10} M_\odot$ should be resolved in all redshift bins of the deep field. We conjecture that very compact galaxies coalesce in the unresolved galaxies in Fig. 7.

4 RESULTS

4.1 Linear regression of size-stellar mass relation

Since the strong correlations of R_{50} and R_{90} with M_* in Figs. 5 and 6 are suggested, we obtain the least square fit between the size and mass of the galaxies with a linear regression,

$$\log R = a_r(\log M_* - M) + \log R_r^M, \quad (3)$$

where r is 50 for half light radius or 90 for 90% light radius and R_r^M is the radius at $M_* = 10^M M_\odot$. M is 10 for all and star-forming galaxies, while $M = 11$ for quiescent galaxies because the quiescent galaxies with $M_* \lesssim 10^{10} M_\odot$ were not observed at $z > 1.5$ and their a_r is statistically less robust due to the small numbers of the sample in narrow mass ranges at high redshifts. We note that quiescent galaxies are located on average below the regression lines in all redshift bins, though the offset is smaller for R_{90} than for R_{50} . The fact suggests that quiescent galaxies are more compact than star-forming galaxies at a give mass. The best-fit slopes (a_{50} and a_{90}) and offsets (R_{50}^M and R_{90}^M) of the regression analysis with mean errors for all, quiescent galaxies (QSG), and star-galaxies (SFG) are summarized in Table 1. The dispersion, σ , of the linear fit is listed in the sixth and last columns. As the exclusion of unresolved sources could biases the results towards larger radii, we obtained in Table 2 the least-squares fit with the unresolved galaxies in Fig. 7.

We depict the evolution of the slope and offset as a function of redshift in Fig. 8. While the slope for the quiescent galaxies are a little steeper than those for star-forming galaxies, the figure indicates that the slopes remain within $\sim 0.1 - 0.2$ and offsets do

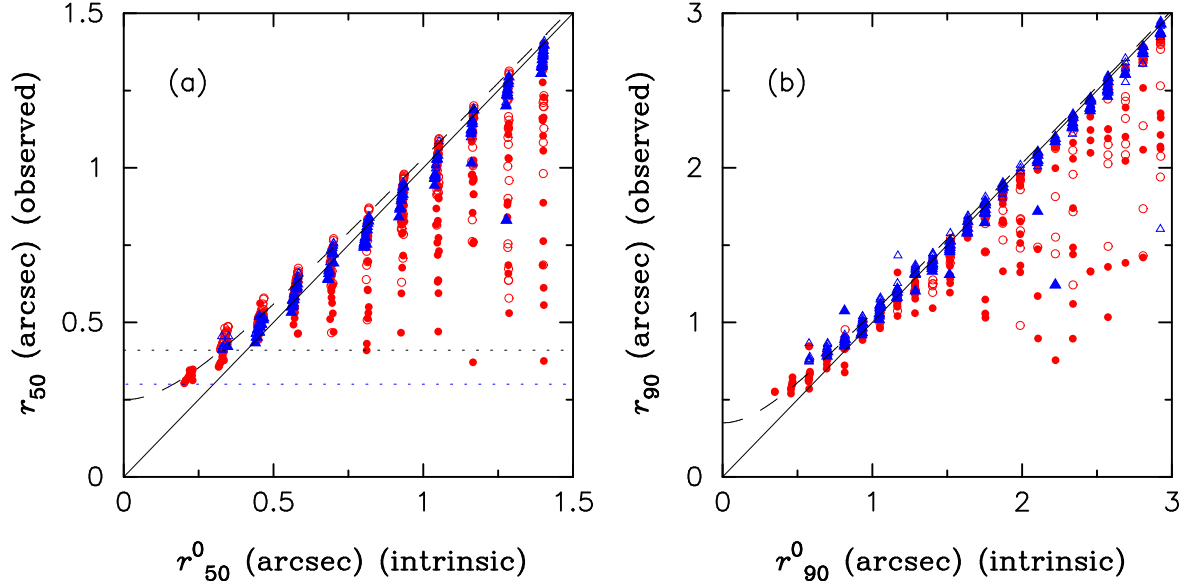


Figure 2. (a) Half-light (r_{50}) and (b) 90 percent-light (r_{90}) radii of mock galaxies embedded in the noise images. The abscissa is the intrinsic values and the ordinate is those observed with SExtractor. Triangles (blue) and circles (red) indicate the model galaxies with exponential and 1/4-law profiles, respectively. Open symbols are the sources ($m_K \leq 25$) in the noise image of the wide field, while filled ones are those ($m_K \leq 26$) in the deep field. The sample galaxies larger than $r_{50} = 0.41$ arcsec for the wide field and $r_{50} = 0.3$ arcsec for the deep field are plotted above horizontal dot lines in (a). The dashed curves show the effect of point spread function $\Delta r = 0.25$ and 0.35 arcsec for r_{50} and r_{90} , respectively.

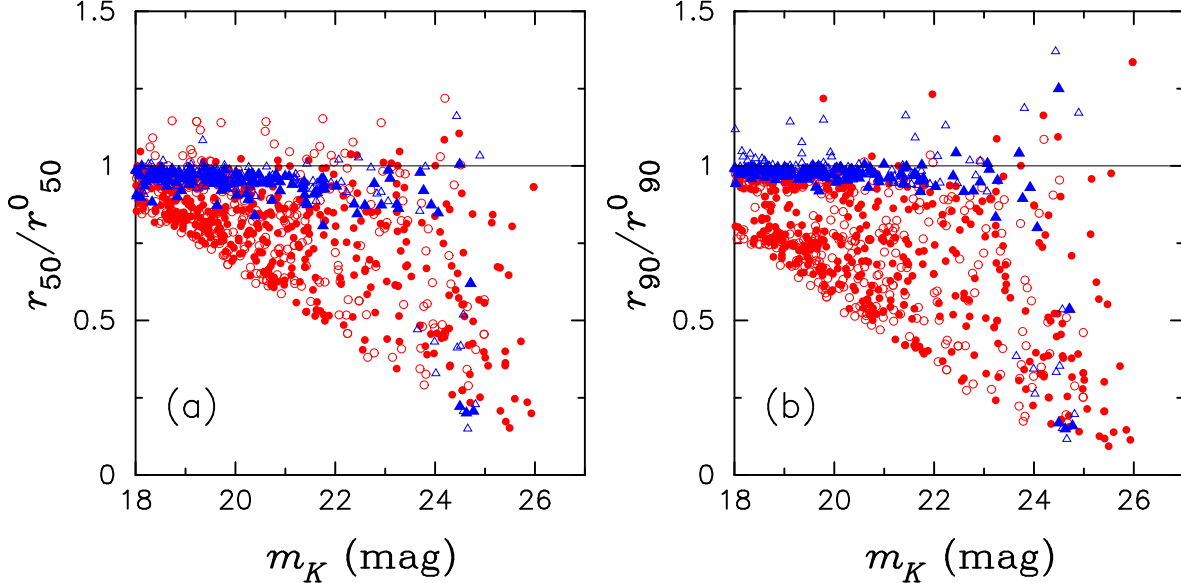


Figure 3. Ratio of observed size to intrinsic for (a) r_{50} and (b) r_{90} as a function of the observed magnitude for mock galaxies. The symbols are the same as in Fig. 2.

not significantly change from $z \sim 3$ to $z \sim 0.3$, irrespective of the sample selection except the quiescent population at $z > 2$ where the statistical error is very large.

For SMSD in Figs. 9 and 10, we define the regression as

$$\mu_* = a_r^\mu \log(M_* - 10) + \mu_r^{10}, \quad (4)$$

where μ_r^{10} is SMSD at $M_* = 10^{10} M_\odot$. The results are shown in Table 3.

4.2 Error estimate

The errors in stellar mass mainly originated from SED fitting and photometric errors of the observations. In the course of χ^2 fitting to obtain the best SED model with various parameters (e.g., star-formation time scale, photometric redshift for galaxies with no spectroscopic redshift available, age, extinction, and metallicity), the probability distributions of stellar mass can be calculated, where the photometry and photometric-redshift errors are included. The error for the observed SMSD is dominated by the error for the

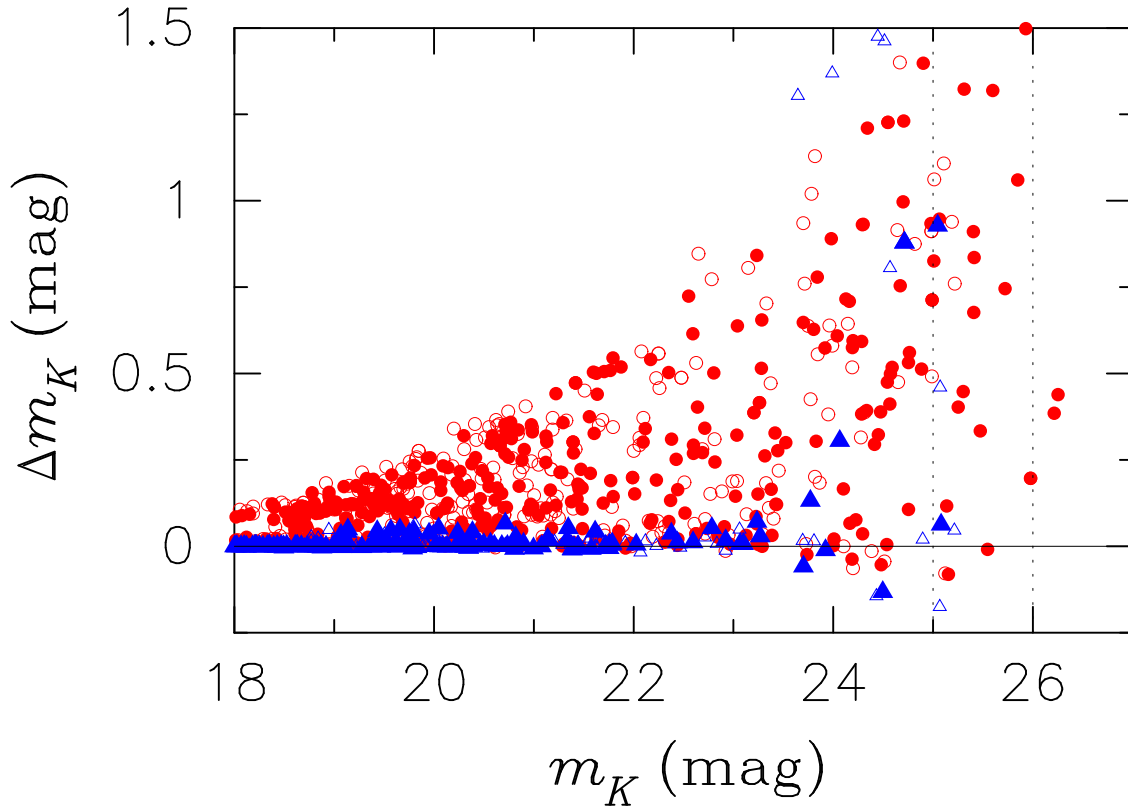


Figure 4. Difference between the intrinsic and observed magnitudes (observed minus intrinsic) as a function of the observed magnitude. The symbols are the same as in Fig. 2.

stellar mass. See more details for the error estimate in K09 and Ichikawa et al. (2010)

The size and magnitude errors in accordance with galaxy magnitude have been examined using mock galaxies (Figs. 3 and 4). If all galaxies have a shape of 1/4-law, the error would be significant. Recalling the size error due to the morphology strongly depends on magnitude, we examine the effect by confining the sample to bright galaxies, where the systematic error becomes smaller. We selected the samples with the magnitude limits, $m_K = 24$ (23), 25(24), 26(25) for the deep (wide) fields, then obtained the regression lines again. The results are compared in Table 3. It should be noted that the section does not change the result.

One would be concerned about the reliance on photometric redshift estimates for high redshift galaxies (e.g., Mosleh et al. 2011). In order to examine the error, we selected only the galaxies with spectroscopic redshift available and compared the result with the photo- z sample. Although the spectroscopic samples are limited to lower redshift, the result does not change our conclusion (Table 3).

Due to possible color gradients in galaxies, it would be best to use images of the same rest-frame band with comparable S/N for measuring the size of galaxies at all redshifts. Nevertheless, we used the radius of galaxies measured on K -band image, because it is deepest among the images we used and because it is the rest-frame optical or longer band at $z \lesssim 3$. If the central region of galaxies are younger (bluer) than the outer region, the mass-weighted radius could be larger than the luminosity-weighted radius. If it is older (redder), the result would be vice versa. Star forming galaxies sometimes show strong morphological variation between observed wavelengths. Bond, Gawiser & Koekemoer (2011) reported that

this was not generically accompanied by a large difference in half-light radius. Barden et al. (2005) measured the disk scale lengths of local galaxies in various bands. The average size is about 10 percent larger in V band than in K band. On the other hand, MacArthur & Courteau (2003) showed the contrary result that the distribution of disc scale lengths was a decreasing trend with increasing wavelengths (see also Cassata et al. 2010 for early-type galaxies at $z \sim 2$).

To investigate the effect of the color gradient, we compare the 90 present-light radius of galaxies measured on the nearest rest-frame V band for each redshift bin. The sizes of the present samples were obtained on ACS I , z , and MOIRCS J , H bands and compared with that of K band in Fig. 11. We used ACS images binned to 0.117 arcsec per pixel, keeping the original image resolution. Fig. 11 demonstrates that the sizes of ACS in I and z bands are systematically ~ 25 percent smaller than that in K band.

The convolution of the ACS I -band image with PSF and seeing enhances low surface brightness details. If the ACS images are convolved with a gaussian (FWHM=2 pixel, 0.234 arcsec), the difference is decreased to ~ 15 percent. As the convolution enhances the galaxy edge of low surface brightness, it tends to give a larger galaxy size (see also fig. 7 of Mancini et al. 2010). It should be noted that the J and H images gives larger image size for smaller galaxies. The size strongly depends on the depth and the seeing size.

4.3 Size evolution

Although we have found the universal relation between M_* and SMSD (or size), which does not depend strongly on redshift, we

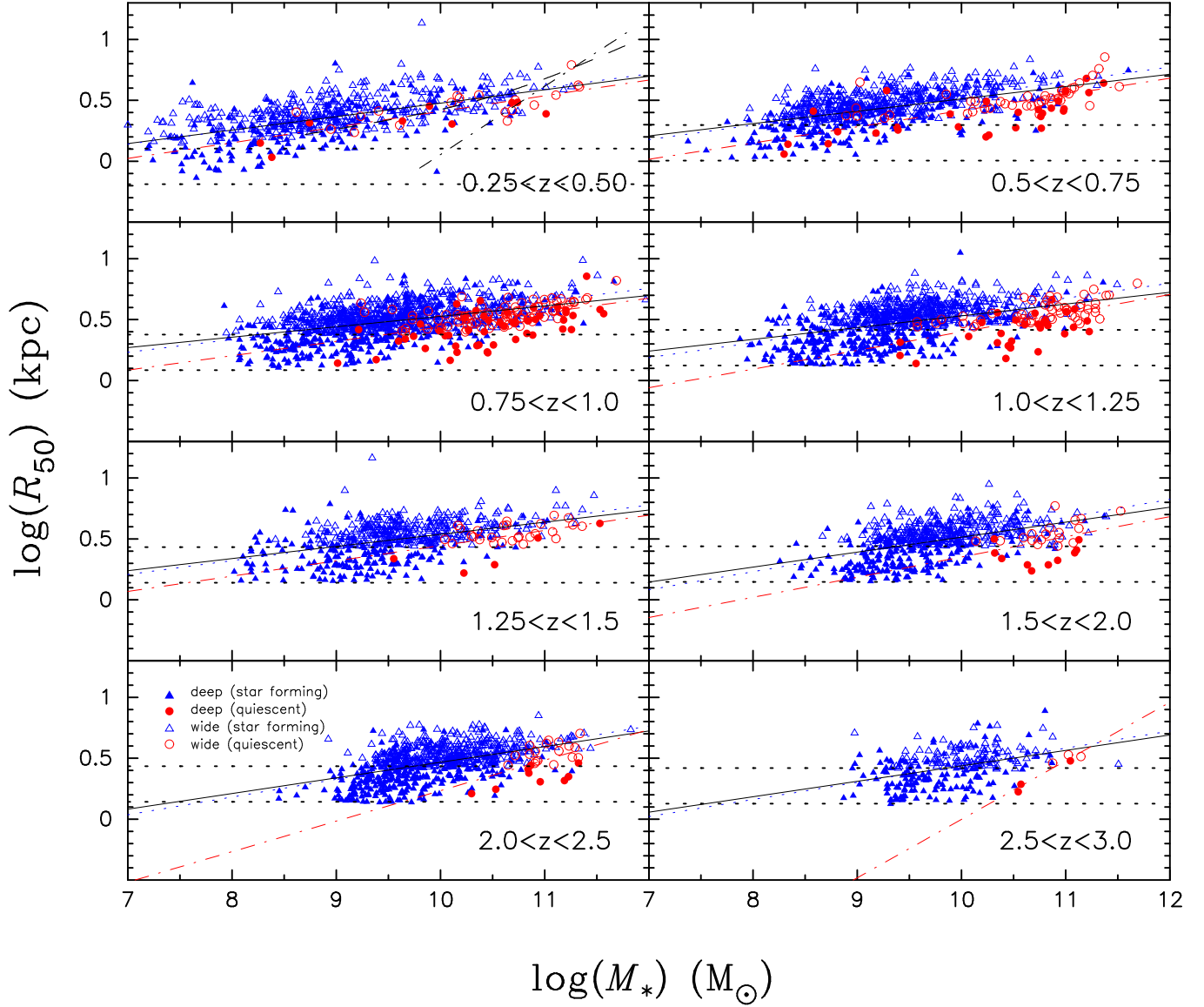


Figure 5. Physical half-light radius (R_{50}), corrected for PSF effects (Eq.1), as a function of the stellar mass (M_*) of the sample galaxies. The galaxies are classified into quiescent (red) and star-forming galaxies (blue) (see text) and the fields (wide and deep) as noted in the bottom left frame. Solid line is the linear regression obtained for all samples in each redshift bin. Red dash-dot and blue dot lines are the regressions for quiescent and star-forming galaxies, respectively. Black dashed and dash-dot lines in the $0.25 < z < 0.5$ bin are the results of effective radius (r_e) for local late- and early-type galaxies (Shen et al. 2003), respectively. The horizontal dot lines are the size limits of the present observation for the wide (upper) and deep (lower) fields at the lower redshift boundary for each redshift bin.

have good reason to expect offsets from the relation for some galaxy populations (e.g., massive compact galaxies) in certain mass and redshift ranges. The regression analysis could be more weighted on the numerous less massive populations. Therefore, it is likely that there are small (but not highly significant) offsets between galaxy populations. The small offsets would account for the size evolution of such populations. Using the M_* - R relation obtained for the galaxies at $0.25 < z < 0.5$ (Tables 1 and 2) as a reference, we examined the deviation of the median size of galaxies in the mass and redshift bins from the reference. The evolution of the massive ($M_* > 10^{10.5} M_\odot$) quiescent galaxies, defined in a $U - V$ and $V - J$ diagram (Williams et al. 2010), is also obtained. (We use median values to avoid unreasonable contributions from outliers with large deviation.) We show the results in Fig. 12, where

unresolved galaxies are included. In addition, the median values of R_{50}/R_{90} , which represent a sort of *compactness* of galaxies, are depicted in the figure to see the evolution of the compactness as a function of redshift. We note that the result with resolved galaxies are in good agreement with that with unresolved galaxies.

5 DISCUSSION

Using the deepest K -band image, we obtained scaling relations between stellar-mass (M_*) and size (or equivalently SMSD) as a function of redshift for galaxies at $0.3 < z < 3$ in a wide mass range of $M_* \sim 10^8 - 10^{11} M_\odot$. We defined the radii encircling half- (R_{50}) and 90 percent-light (R_{90}) in a circular aper-

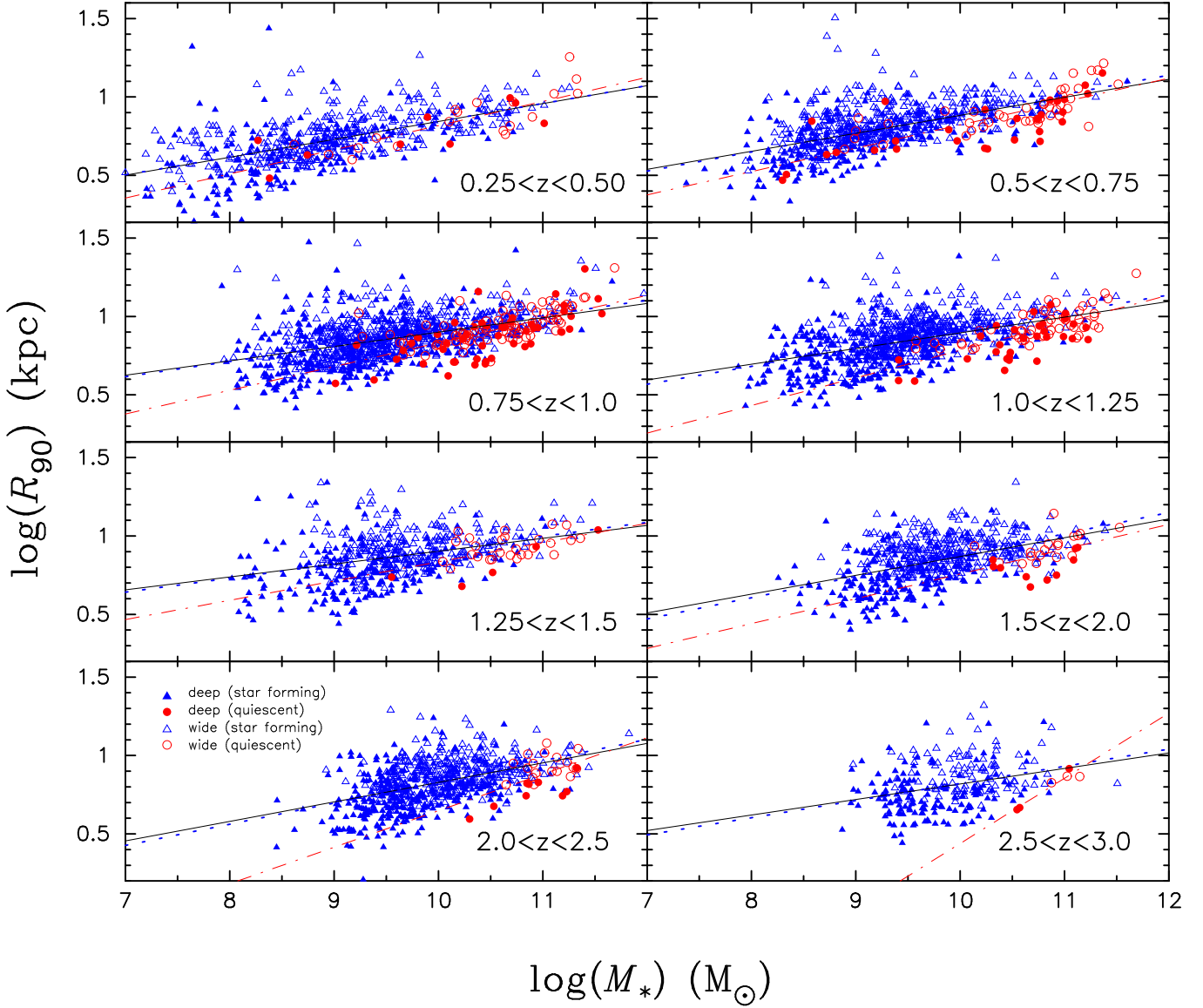


Figure 6. Same as Fig. 5, but for 90 percent-light radius (R_{90}).

ture. The depth was found to be crucial for proper measure of the size and mass for less massive galaxies dimmed due to cosmic expansion. We conclude that there is no strong evidence for the size evolution at a given mass over the redshift range, irrespective of galaxy populations (star-forming, quiescent). The size-mass relation ($R \propto M_*^\alpha$) have a universal slope ($\alpha \sim 0.1 - 0.2$) and small offsets ($\lesssim 50$ percent). In other words, as galaxies grow in mass through star formation or merging process, their sizes evolve in such a way that galaxies in general move along the scaling relation. The universal relation demonstrates that the stellar mass in galaxies with the same stellar mass was built up on average in a similar manner over cosmic times. The trend is insensitive to the stellar populations. Our result is comparable with the $r_e \propto M_*^{0.15}$ found by Shen et al. (2003) for low-mass galaxies ($M_* < 10^{10.6} M_\odot$). On the other hand, it is in contrast to the steeper relation for massive galaxies obtained by previous studies (e.g., Shen 2003; Bernardi et al. 2011). The scaling relations are much tighter ($\sigma \sim 0.12-0.17$ dex) than those ($\sigma \sim 0.3-0.5$ dex) of previous studies in the local

universe (e.g., Shen et al. 2003) or at high redshifts (e.g., Franx et al. 2008).

The weak growth of the galaxy size, irrelevant to galaxy mass, is in disagreement with the scenario that more massive galaxies rapidly changed their sizes. If massive high- z galaxies are several times smaller than local galaxies with comparable mass, they should be located well above the stellar mass vs. SMSD relations. Several candidates of such compact galaxies with $M_* > 10^{11}$ possibly coalesce as unresolved galaxies in Figs. 9 and 10. However, such galaxies are found to be few. Our finding is in contrast with the previous results for quiescent early-type massive galaxies (e.g., Zirm et al. 2007; Williams et al. 2010). With regard to SMSD, the average SMSDs in R_{50} for our sample galaxies with $M_* > 10^{10} M_\odot$ are found not to evolve with redshift ($\log \mu_{R_{50}} = 8.53 - 8.70$). The average SMSD for all galaxies at $0.25 < z < 3.0$ is 8.60 ± 0.01 , which is very consistent with the result, 0.85 ± 0.03 , for disk galaxies with $M_* > 10^{10}$ obtained by Barden et al (2005), though our sample could be a mixture of disk and elliptical galax-

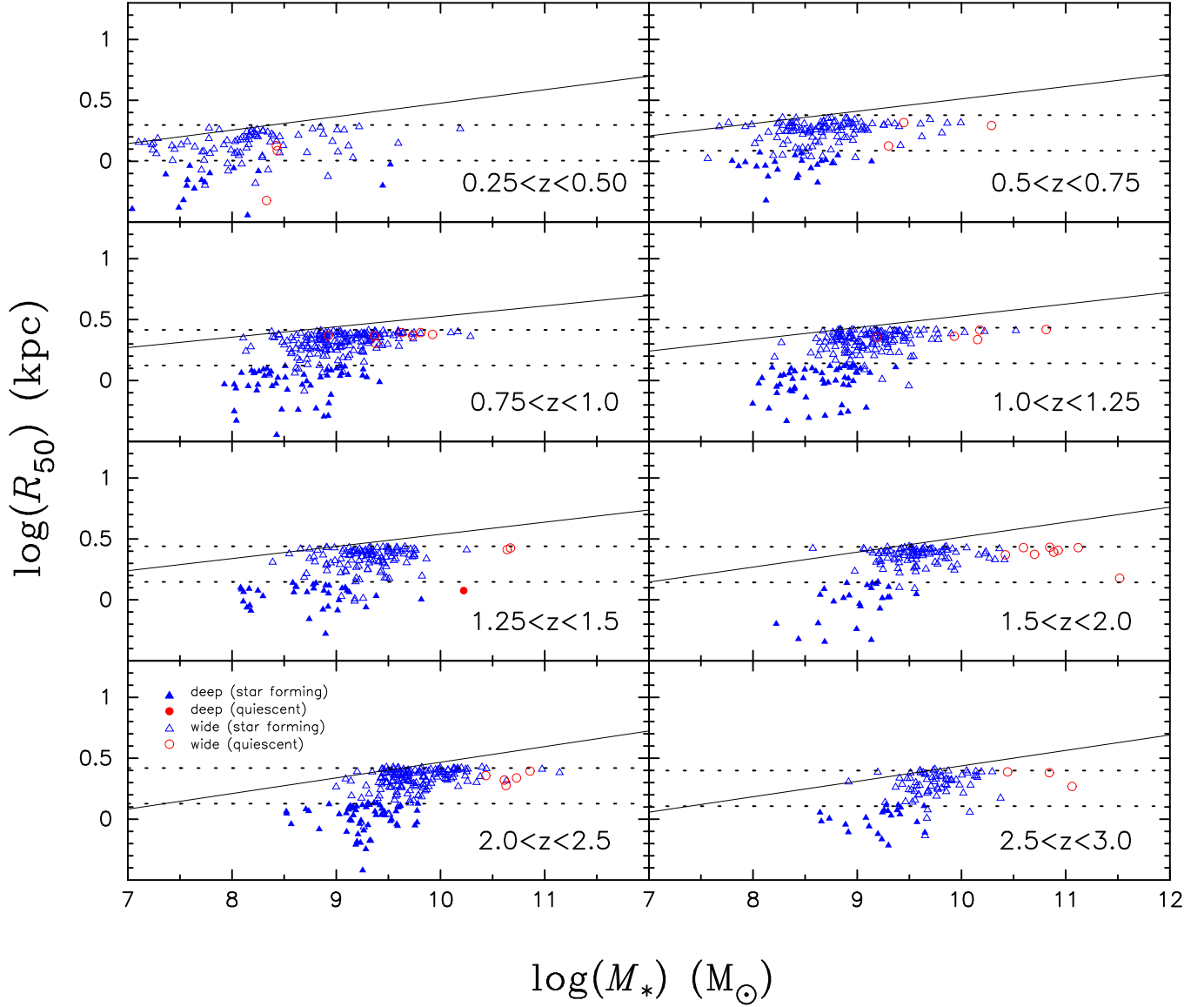


Figure 7. Same as Fig. 5, but for unresolved galaxies. The same regression lines for all sample in each redshift bin as in Fig. 5 are shown for reference. The dotted lines are the size limits for the wide (upper) and deep (lower) fields at the upper redshift boundary for each redshift bin.

ies. However, due to small volume of the present study, the results could be subject to statistical uncertainties.

The weak size evolution presented in the present study is reconciled with the surface brightness (SB) evolution. Ichikawa et al. (2010) presented a universal linear correlation between the stellar mass and SB in rest-frame V and z bands for galaxies at $0.3 < z < 3$, using the same sample as the present study. The correlation has a nearly constant slope, independent of redshift and color of galaxies in the rest- z frame. In contrast, SB shows a strong dependence on redshift for a given stellar mass. It evolves as $(1+z)^{-2.0 \sim -0.8}$. The increase in the luminosity with redshift is estimated by using the expected luminosity evolution from a single burst at $z = 4$ for massive galaxies ($M_* > 10^{10}$) and constant star formation for blue samples ($U - V < 0$) for less massive galaxies. The redshift dependence of SB evolution is well explained by the pure luminosity evolution of galaxies out to $z \sim 3$ without the need of the size evolution, which supports the results for young

early-type galaxies (e.g., Saracco et al. 2011) and for disk galaxies at $z \lesssim 1$ (Barden et al. 2005).

Nevertheless, there are some populations having a small offset from the universal scaling relation. We see more or less evolution in the size and compactness for such populations as a function of redshift in Fig. 12. The figure suggests a moderate increase of 30–50 percent for R_{50} and R_{90} for less massive galaxies ($M_* < 10^{10} M_\odot$) from $z \sim 3$ to $z \sim 1$, while the sizes remains unchanged or slightly decrease towards $z \sim 0.3$. For massive galaxies ($M_* \gtrsim 10^{11} M_\odot$), the evolution is $\sim 70 - 80$ percent in R_{90} from $z \sim 3$ to $z \sim 0.3$, though that in R_{50} is weaker. R_{90} evolved as $\propto (1+z)^{-0.5}$. It is noted that Trujillo et al. (2006), using the ground-based K -band data comparable with our depth, but in a smaller region (6.3 arcmin²), concluded that there was no evidence for significant evolution for the size-mass relation and that there was small increase (29 percent) since $z \sim 2.5$ for the most massive bin $M_* > 4 \times 10^{10} M_\odot$. In our sample, the average R_{50} for the most massive bin of $M_* = 10^{11} - 10^{12} M_\odot$ is larger

Table 1. Linear fit of radius to stellar mass for resolved galaxies.

Redshift	Sample	R_{50}				R_{90}			
		N	a_{50}	$\log R_{50}^M$ (kpc)	σ	N	a_{90}	$\log R_{90}^M$ (kpc)	σ
$0.25 \leq z < 3.00$	all	5259	0.101 ± 0.002	0.508 ± 0.002	0.130	5236	0.103 ± 0.003	0.874 ± 0.002	0.148
	QSG	408	0.126 ± 0.009	0.543 ± 0.007	0.110	408	0.143 ± 0.008	0.955 ± 0.006	0.099
	SFG	4851	0.113 ± 0.003	0.520 ± 0.002	0.129	4828	0.108 ± 0.003	0.880 ± 0.003	0.151
$0.25 \leq z < 0.50$	all	543	0.111 ± 0.006	0.477 ± 0.009	0.133	542	0.114 ± 0.008	0.844 ± 0.011	0.168
	QSG	28	0.129 ± 0.020	0.537 ± 0.026	0.098	28	0.154 ± 0.021	0.971 ± 0.027	0.100
	SFG	515	0.115 ± 0.007	0.486 ± 0.010	0.133	514	0.114 ± 0.009	0.845 ± 0.012	0.170
$0.50 \leq z < 0.75$	all	717	0.101 ± 0.006	0.511 ± 0.006	0.119	714	0.115 ± 0.006	0.883 ± 0.006	0.124
	QSG	70	0.133 ± 0.018	0.548 ± 0.019	0.126	70	0.149 ± 0.015	0.970 ± 0.016	0.107
	SFG	647	0.119 ± 0.007	0.535 ± 0.007	0.113	644	0.122 ± 0.007	0.894 ± 0.008	0.124
$0.75 \leq z < 1.00$	all	1083	0.086 ± 0.005	0.527 ± 0.004	0.123	1079	0.091 ± 0.006	0.900 ± 0.005	0.151
	QSG	134	0.118 ± 0.017	0.558 ± 0.012	0.104	134	0.151 ± 0.015	0.983 ± 0.011	0.095
	SFG	949	0.105 ± 0.006	0.547 ± 0.005	0.121	945	0.098 ± 0.007	0.908 ± 0.006	0.156
$1.00 \leq z < 1.25$	all	888	0.097 ± 0.006	0.531 ± 0.005	0.130	885	0.100 ± 0.006	0.895 ± 0.005	0.124
	QSG	83	0.153 ± 0.024	0.553 ± 0.014	0.105	83	0.176 ± 0.019	0.960 ± 0.011	0.085
	SFG	805	0.122 ± 0.007	0.554 ± 0.006	0.128	802	0.114 ± 0.007	0.909 ± 0.006	0.125
$1.25 \leq z < 1.50$	all	519	0.100 ± 0.008	0.538 ± 0.006	0.127	514	0.082 ± 0.011	0.903 ± 0.008	0.161
	QSG	32	0.125 ± 0.037	0.570 ± 0.020	0.089	32	0.123 ± 0.033	0.958 ± 0.018	0.079
	SFG	487	0.114 ± 0.009	0.550 ± 0.007	0.127	482	0.089 ± 0.012	0.909 ± 0.009	0.165
$1.50 \leq z < 2.00$	all	555	0.123 ± 0.010	0.514 ± 0.006	0.128	554	0.120 ± 0.010	0.869 ± 0.006	0.128
	QSG	28	0.166 ± 0.074	0.518 ± 0.027	0.121	28	0.158 ± 0.058	0.916 ± 0.021	0.094
	SFG	527	0.148 ± 0.010	0.528 ± 0.006	0.124	526	0.136 ± 0.011	0.878 ± 0.006	0.128
$2.00 \leq z < 2.50$	all	700	0.128 ± 0.009	0.468 ± 0.005	0.121	696	0.124 ± 0.010	0.829 ± 0.006	0.146
	QSG	27	0.250 ± 0.083	0.484 ± 0.021	0.109	27	0.233 ± 0.074	0.881 ± 0.019	0.097
	SFG	673	0.146 ± 0.009	0.473 ± 0.005	0.119	669	0.135 ± 0.011	0.832 ± 0.006	0.147
$2.50 \leq z < 3.00$	all	254	0.127 ± 0.017	0.438 ± 0.008	0.130	252	0.099 ± 0.022	0.818 ± 0.011	0.166
	QSG	6	0.480 ± 0.070	0.479 ± 0.019	0.040	6	0.416 ± 0.062	0.855 ± 0.017	0.035
	SFG	248	0.140 ± 0.018	0.442 ± 0.009	0.129	246	0.109 ± 0.024	0.822 ± 0.011	0.167

by $\sim 20 - 30$ percent at $z \sim 0.3$ than at $z \sim 2.5$, which is in good agreement with the result of Trujillo et al. (2006), whereas it is much weaker than those of other studies for galaxies of similar mass (e.g., Franx et al. 2008; Buitrago et al. 2008; van der Wel et al. 2009; Williams et al. 2010). Using new deep WFC3 data, Casata et al. (2011) and Law et al. (2012) have given new evidences of compact galaxies at high- z . Although the data in H band is shallower by $1 \text{ mag arcsec}^{-2}$ than our K -band data, their conclusion would be robust. It would be possible that the compact galaxies are mingled in unresolved galaxies of the present sample or that the difference of the definition for half-right radius (r_e and r_{50}) gives the contradict result.

The ratio, R_{50}/R_{90} , in Fig. 12 would give a clue to understanding the evolution of the compactness of galaxies. While middle and low mass galaxies shows no evolution in the compactness, the galaxies in the most massive bin are more compact at higher redshift. Recalling weaker evolution in R_{50} than in R_{90} , we infer that the compactness evolution is ascribed mainly to the expansion of the outer rim of massive galaxies. In other words, at a given mass, massive galaxies in the local universe are more influenced by mergers or star formation at the outer envelopes than those at high redshifts. It would be worth noting that the galaxies in the massive bin of the deep field are complete in sampling over the present redshift range and their R_{50} and R_{90} are well resolved in the present PSF. However, the present observation samples a comparatively small volume and therefore, the results could be subject to statistical uncertainties for massive galaxies of low number density due to field variances.

The size evolution is often used to advocate the merging processes in the hierarchical paradigm of galaxy formation and evolution. Minor dry merger is a plausible mechanism for weak size evolution (e.g., Guo & White 2008; Bezanson et al. 2009; Naab, Johansson, & Ostriker 2009; Hopkins et al. 2010). In that the size evolution is stronger in massive galaxies, our findings are qualitatively in agreement with previous studies based on simulations (e.g., Boylan-Kolchin, Ma, & Quataert 2006; Hopkins et al. 2009a). Naab et al. (2009) showed that minor mergers or the accretion of relatively low-mass satellites may be the main driver for the late evolution of sizes of massive early-type galaxies. Somerville et al. (2008) showed based on a CDM model of disc formation with $M_* > 10^{10} M_\odot$ that the average size of discs at fixed stellar mass was about 50 percent larger than that at $z \sim 3$. The predicted evolution in the mean size at a fixed stellar mass since $z \sim 1$ is about $15 \sim 20$ percent, which is comparable with our observations.

The newly accreted small galaxies preferentially populate the outer region of massive galaxies. The small size growth of the present result is plausibly accounted for by minor mergers or the accretion of relatively low-mass satellites (e.g., Naab et al. 2009; Hopkins et al. 2009a). Naab et al. (2009) and Fan et al. (2010) showed the fractional variation of the gravitational radius of the main galaxy after N minor-merger events with $R \propto M_*^\alpha$ as

$$\frac{r_f}{r_i} = \left\{ \frac{(1+\eta)^2}{1+\eta^{2-\alpha}} \right\}^N, \quad (5)$$

where r_f and r_i are final and initial galaxy sizes, η is the fractional ratio of merging galaxy to the main galaxy. It takes ~ 1 (~ 3) minor-

Table 2. Linear fit of radius to stellar mass with unresolved galaxies

Redshift	Sample	R_{50}				R_{90}			
		N	a_{50}	$\log R_{50}^M$ (kpc)	σ	N	a_{90}	$\log R_{90}^M$ (kpc)	σ
$0.25 \leq z < 3.00$	all	6532	0.131 ± 0.003	0.484 ± 0.002	0.161	6502	0.125 ± 0.003	0.852 ± 0.002	0.161
	QSG	445	0.132 ± 0.008	0.536 ± 0.007	0.116	445	0.147 ± 0.008	0.946 ± 0.006	0.108
	SFG	6087	0.144 ± 0.003	0.497 ± 0.003	0.162	6057	0.130 ± 0.003	0.859 ± 0.003	0.164
$0.25 \leq z < 0.50$	all	646	0.136 ± 0.007	0.475 ± 0.010	0.156	645	0.133 ± 0.008	0.838 ± 0.012	0.181
	QSG	31	0.165 ± 0.023	0.554 ± 0.034	0.129	31	0.180 ± 0.022	0.983 ± 0.033	0.124
	SFG	615	0.141 ± 0.007	0.485 ± 0.011	0.156	614	0.133 ± 0.008	0.841 ± 0.013	0.183
$0.50 \leq z < 0.75$	all	858	0.128 ± 0.006	0.503 ± 0.007	0.136	855	0.137 ± 0.006	0.875 ± 0.007	0.134
	QSG	73	0.137 ± 0.017	0.546 ± 0.019	0.127	73	0.155 ± 0.015	0.968 ± 0.016	0.111
	SFG	785	0.150 ± 0.007	0.532 ± 0.008	0.133	782	0.149 ± 0.007	0.890 ± 0.008	0.135
$0.75 \leq z < 1.00$	all	1313	0.129 ± 0.006	0.512 ± 0.005	0.155	1308	0.125 ± 0.006	0.886 ± 0.005	0.161
	QSG	141	0.119 ± 0.015	0.557 ± 0.012	0.102	141	0.158 ± 0.014	0.984 ± 0.011	0.094
	SFG	1172	0.152 ± 0.007	0.536 ± 0.006	0.157	1167	0.135 ± 0.007	0.898 ± 0.007	0.166
$1.00 \leq z < 1.25$	all	1082	0.142 ± 0.007	0.516 ± 0.006	0.164	1077	0.129 ± 0.006	0.881 ± 0.006	0.146
	QSG	88	0.150 ± 0.022	0.550 ± 0.013	0.103	88	0.171 ± 0.018	0.958 ± 0.011	0.084
	SFG	994	0.174 ± 0.008	0.546 ± 0.007	0.164	989	0.146 ± 0.007	0.898 ± 0.007	0.148
$1.25 \leq z < 1.50$	all	675	0.145 ± 0.010	0.515 ± 0.008	0.159	668	0.120 ± 0.011	0.879 ± 0.009	0.176
	QSG	35	0.152 ± 0.045	0.562 ± 0.025	0.111	35	0.141 ± 0.037	0.951 ± 0.020	0.091
	SFG	640	0.163 ± 0.011	0.530 ± 0.009	0.160	633	0.130 ± 0.012	0.887 ± 0.010	0.179
$1.50 \leq z < 2.00$	all	685	0.166 ± 0.012	0.487 ± 0.007	0.174	684	0.133 ± 0.009	0.847 ± 0.006	0.139
	QSG	36	0.077 ± 0.069	0.475 ± 0.024	0.128	36	0.044 ± 0.064	0.865 ± 0.023	0.120
	SFG	649	0.206 ± 0.013	0.509 ± 0.008	0.171	648	0.159 ± 0.010	0.860 ± 0.006	0.138
$2.00 \leq z < 2.50$	all	923	0.187 ± 0.009	0.428 ± 0.005	0.152	918	0.165 ± 0.010	0.796 ± 0.005	0.156
	QSG	32	0.281 ± 0.068	0.477 ± 0.019	0.103	32	0.284 ± 0.062	0.870 ± 0.017	0.094
	SFG	891	0.208 ± 0.010	0.436 ± 0.005	0.151	886	0.179 ± 0.011	0.801 ± 0.005	0.157
$2.50 \leq z < 3.00$	all	350	0.183 ± 0.017	0.400 ± 0.009	0.150	347	0.139 ± 0.020	0.779 ± 0.010	0.175
	QSG	9	0.251 ± 0.133	0.433 ± 0.039	0.097	9	0.157 ± 0.148	0.799 ± 0.043	0.109
	SFG	341	0.206 ± 0.018	0.409 ± 0.009	0.149	338	0.156 ± 0.022	0.786 ± 0.010	0.176

Table 3. Linear fit of surface mass density of galaxies in $0.25 < z < 3.0$.

Selection ^a	Sample	R_{50}				R_{90}			
		N	a_{50}^μ	μ_{50}^{10} ($M_\odot \text{ kpc}^{-2}$)	σ	N	a_{90}^μ	μ_{90}^{10} ($M_\odot \text{ kpc}^{-2}$)	σ
$m_K \leq 26(25)$	all	5259	0.80 ± 0.00	8.19 ± 0.00	0.26	5236	0.79 ± 0.01	7.71 ± 0.00	0.30
	QSG	408	0.75 ± 0.02	8.37 ± 0.01	0.22	408	0.71 ± 0.02	7.83 ± 0.01	0.20
	SFG	4851	0.77 ± 0.01	8.16 ± 0.00	0.26	4828	0.78 ± 0.01	7.70 ± 0.01	0.30
with unresolved galaxies	all	6532	0.74 ± 0.01	8.23 ± 0.00	0.32	6502	0.75 ± 0.01	7.75 ± 0.00	0.32
	QSG	445	0.74 ± 0.02	8.39 ± 0.01	0.23	445	0.71 ± 0.02	7.86 ± 0.01	0.22
	SFG	6087	0.71 ± 0.01	8.21 ± 0.01	0.32	6057	0.74 ± 0.01	7.74 ± 0.01	0.33
$m_K \leq 25(24)$		3980	0.80 ± 0.01	8.19 ± 0.00	0.25	3972	0.80 ± 0.01	7.71 ± 0.00	0.28
$m_K \leq 24(23)$		2378	0.82 ± 0.01	8.20 ± 0.01	0.25	2378	0.79 ± 0.01	7.71 ± 0.00	0.23
spectroscopic redshift		1610	0.81 ± 0.01	8.16 ± 0.01	0.24	1610	0.77 ± 0.01	7.69 ± 0.01	0.22

^a) Selection for the deep field (parentheses are the sample for the wide field)

merger events with $\alpha = 0.15$ to increase the radius by ~ 20 (~ 70) percent for massive galaxies since $z \sim 3$, provided that the merger mass ratio is 1:10. It would not be unreasonable that massive galaxies experienced such a small number of minor merging since $z \sim 3$ (e.g., Bundy et al. 2009; López-Sanjuan et al. 2011).

Deep observations will be important in constraining the exact amount (or lack thereof) and distribution of merging galaxies, and how galaxies built up with redshift. In this context, our finding demonstrates that minor mergers in massive system built up an envelope of lower surface density materials. Deeper imaging ob-

servations in a wider field with high spatial resolution and consistent analyses from the local universe to high redshift will give constraints on the compactness and the amount of low-surface brightness material at the outer envelope as a function of redshift to improve our understanding of galaxy formation.

ACKNOWLEDGMENTS

This work has been supported in part by a Grant-in-Aid for Scientific Research (21244012) of the Ministry of Education, Culture,

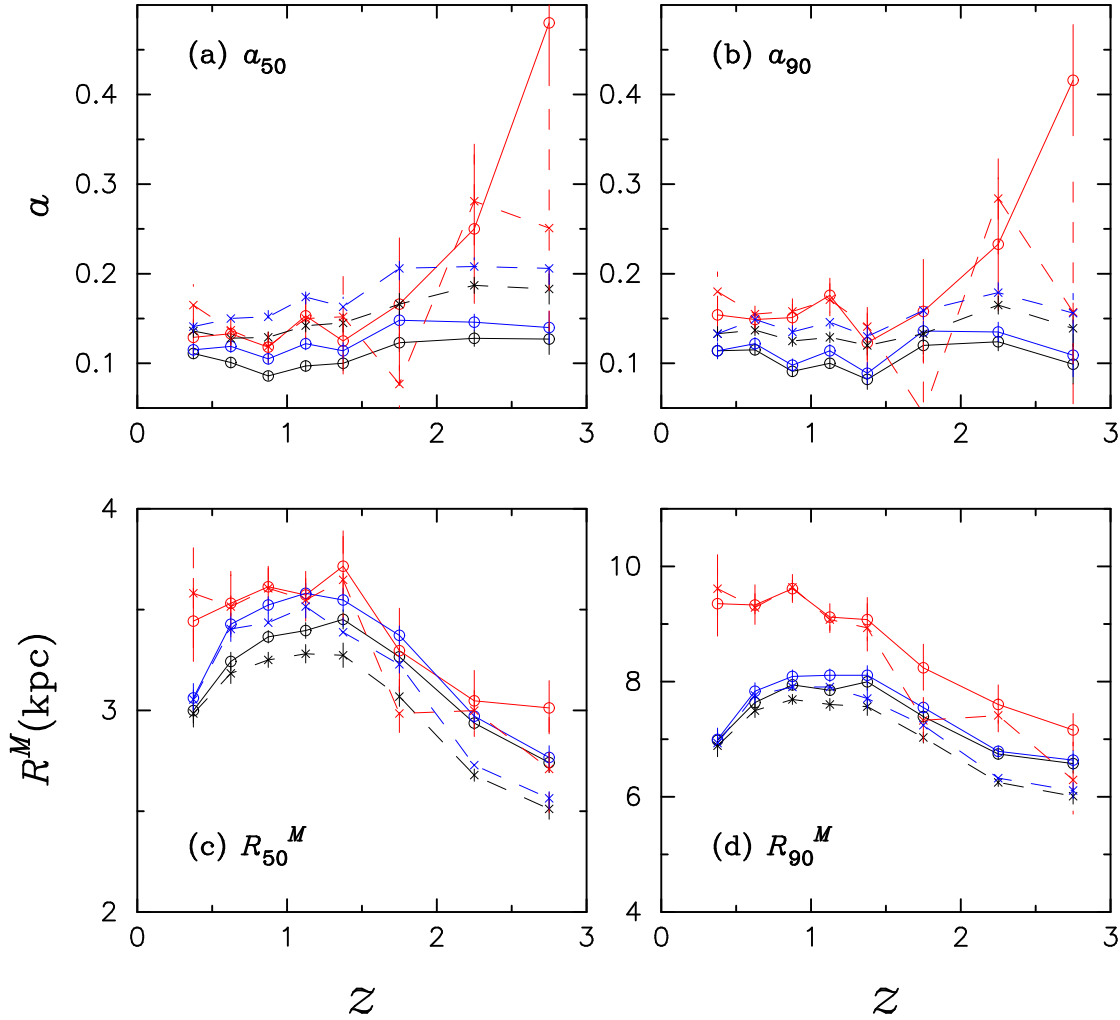


Figure 8. Evolution of the slope and offset (Tables 2 and 3) as a function of redshift. Circles with solid line and crosses with dashed lines are the results for resolved galaxies and those with unresolved galaxies. Black, red, and blue symbols are the samples for all, quiescent, and star-forming galaxies, respectively.

Sports, Science and Technology in Japan. We thank Ramsey Lundock for careful reading of the manuscript. MODS catalogue has been accomplished by MOIRCS builders. We owe the present study to their dedicated efforts.

REFERENCES

- Akiyama M., Minowa Y., Kobayashi N., Ohta K., Ando M., and Iwata I. 2008, *ApJS*, 175, 1
- Barden A., et al. 2005, *ApJ*, 635, 959
- Bernardi M., Roche N., Shankar F., Steth, R. K., 2011, *MNRAS*, 412, L6
- Bertin E., Arnouts S. 1996, *A&AS*, 117, 393
- Bezanson R., van Dokkum P. G., Tal T., Marchesini D., Kriek M., Franx M., Coppi P., *ApJ*, 697, 1290
- Bond N. A., Gawiser E., Koekemoer A. M., 2011, *ApJ*, 729, 48
- Bouwens R. J., Illingworth G. D., Blakeslee J. P., Broadhurst T. J., Franx M., 2004, *ApJ*, 611, L1
- Boylan-Kolchin M., Ma C-P., Quataert E., 2006, *MNRAS*, 369, 1081
- Bruzual G., Charlot S. 2003, *MNRAS*, 344, 1000
- Buitrago F., Trujillo I., Conselice C. J., Bouwens R. J., Dickinson M., Yan H., 2008, *ApJ*, 687, L61
- Bundy K., Fukugita M., Ellis R. S., Targett T. A., Belli S., Kodama T., *ApJ*, 697, 1369
- Carrasco E. R., Conselice C. J., Trujillo I., 2010, *MNRAS*, 405, 2253
- Cassata P., et al., 2010, *ApJ*, 714, L79
- Cassata P., et al., 2011, *ApJ*, 743, 96
- Cimatti A., et al. 2008, *A&A*, 482, 21
- Daddi E., et al. 2005, *ApJ*, 626, 680
- Damjanov I., et al., 2009, *ApJ*, 695, 101
- Fan L., Lapi A., de Zotti G., Danese L., 2008, *ApJ*, 689, L101
- Fan L., Lapi A., Bressan A., Bernardi M., de Zotti G., Danese L., 2010, *ApJ*, 718, 1460
- Fontana A., et al. 2009, *A&A*, 501, 15
- Franx M., van Dokkum P. G., Schreiber M. F., Wuyts S., Labbé, Toft S., 2008, *ApJ*, 688, 770
- Fukugita M., Ichikawa T., Gunn J. E., Doi M., Shimasaku K., Schneider D. P. 1996, *AJ*, 111, 1748
- Guo Q. White S. D. M., 2008, *MNRAS*, 384, 2
- Hopkins P. F., Hernquist, L., Cox T. J., Keres, D., Wuyts S., 2009, *ApJ*, 691, 1424

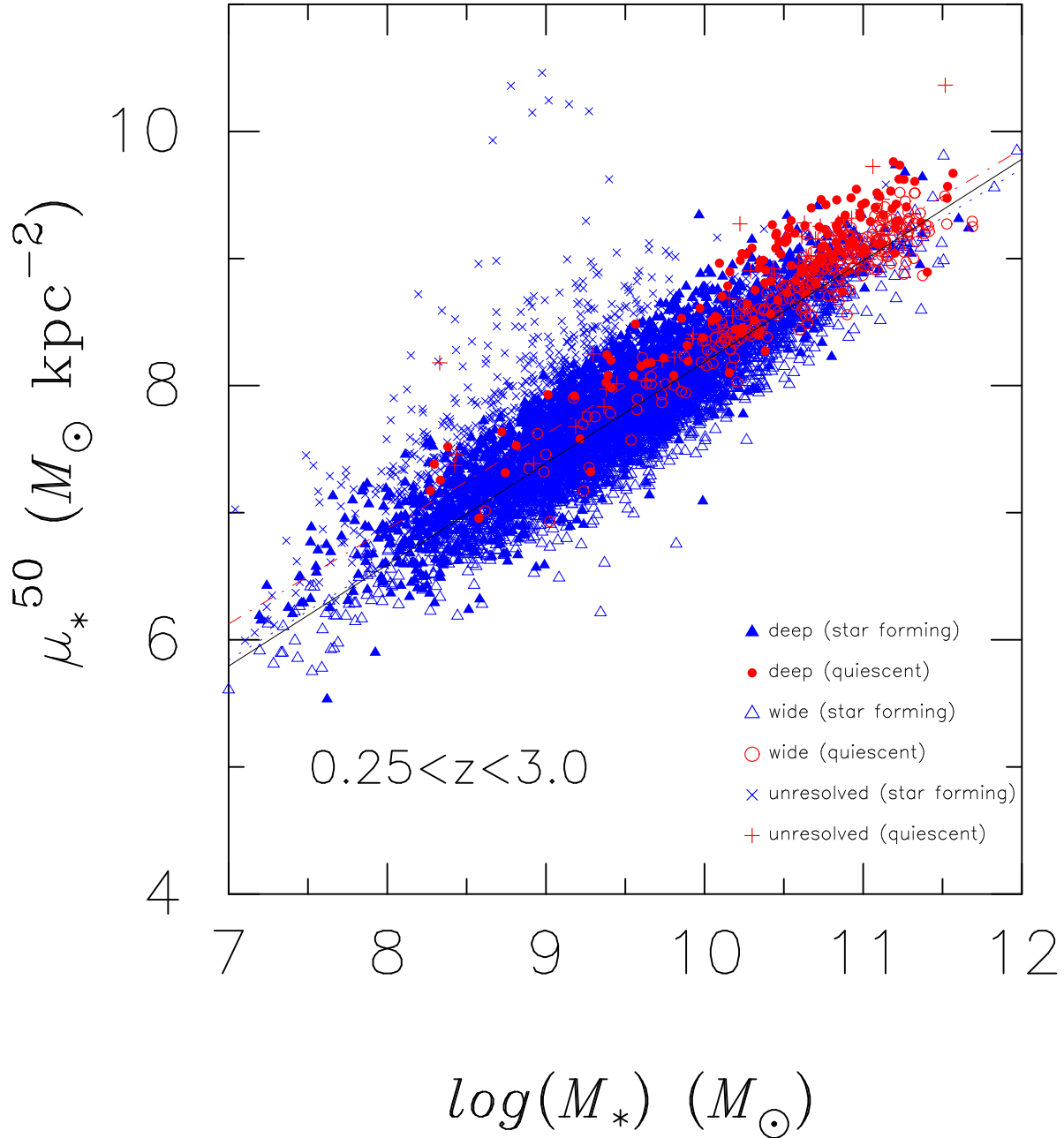


Figure 9. Correlation of stellar-mass surface density (μ_*) in half-light radius (R_{50}) with stellar mass (M_*) of the sample galaxies in $0.3 < z < 3$. The notation of symbols are the same as in Fig. 5. Red pluses and blue crosses show unresolved quiescent and star-forming galaxies, respectively. Solid (black), dash-dot (red), and dot (blue) lines are the linear fits for the resolved all, quiescent, and star-forming galaxies.

Hopkins P. F., Bundy K., Murray N., Quataert E., Lauer T. R., and Ma, C.-P., 2009, MNRAS, 398, 898
 Hopkins P. F., Bundy K., Hernquist L., Wuyts S., Cox T. J., MNRAS, 401, 1099
 Ichikawa T., Kajisawa M., Yamada T., Akiyama M., Yoshikawa T., Onodera M., Konishi M., 2010, ApJ, 709, 741
 Kajisawa M., et al., 2009, ApJ, 702, 1393
 Kajisawa M., et al., 2011, PASJ, 63, S379
 Kajisawa M., Yamada T., 2001, PASJ, 53, 833
 Konishi M., et al., 2011, PASJ, 63, S363
 Law, D. R., Steidel, D. C., Shapley, A. E., Nagy, S. R., Reddy, N. A., Erb, D. K., 2012, ApJ, 745, 85

López-Sanjuan C., et al. 2011, A&A, 530, A20
 MacArthur L. A., Courteau S., 2003, ApJ, 582, 689.
 Mancini C., et al., 2010, MNRAS, 401, 933
 McIntosh D., et al., 2005, ApJ, 632, 191
 Mosleh M., Williams R. J., Franx M., Kriek, M., 2011, ApJ, 727, 5
 Naab T., Johansson P. H., Ostriker J. P., 2009, ApJ, 699, L178
 Nagy S. R., Law D. R., Shapley A. E., Steidel C. C., 2011, ApJ, 735, 19L
 Oke J. B., Gunn J. E. 1983, ApJ, 266, 713
 Saracco P., Longhetti M., Andreon S., 2011, MNRAS, 392, 718
 Saracco P., Longhetti M., Gargiulo A., 2011, MNRAS, 412, 2707

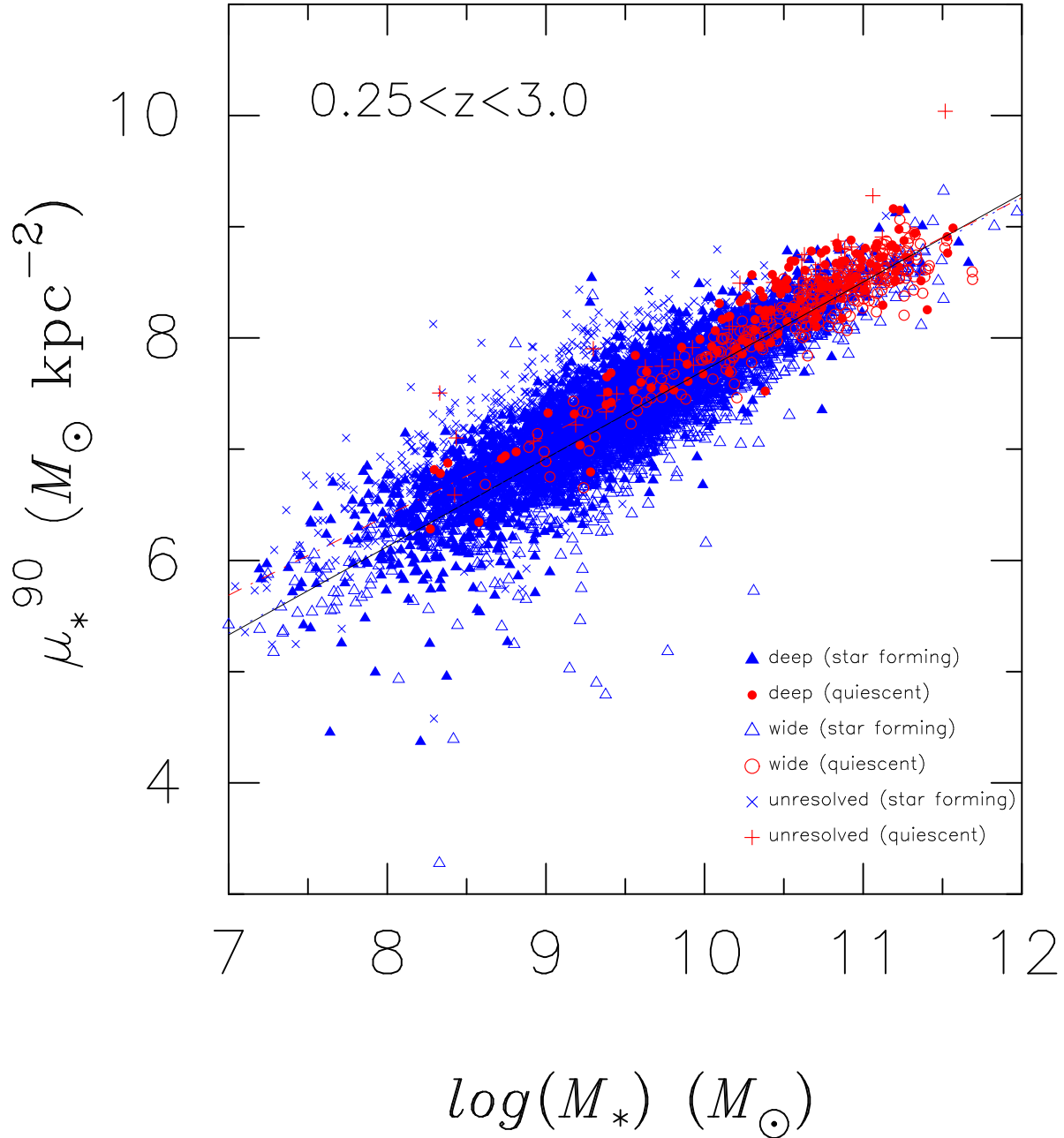


Figure 10. Same as Fig. 9, but for 90 percent-light radius (R_{90}).

Sérsic J.-L. 1968, *Atlas de Galaxias Australes* (Cordoba: Obs. Astron.)

Somerville R. S., et al. 2008, *ApJ*, 672, 776

Szomoru D., 2010, *ApJ*, 714, L244

Stott J. P., Collins C. A., Burke C., Hamilton-Morris V., Smith G. P., 2011, *MNRAS*, 414, 445

Shen S., Mo H. J., White S. D. M., Blanton M. R., Kauffmann G., Voges W., Brinkmann J., Csabai I., 2003, *MNRAS*, 343, 978

Stockton A., Shih H.-Y., Larson K., 2010, *ApJ*, 709, L58

Suzuki R., et al. 2008, *PASJ*, 60, 1347

Toft S., et al., 2007, *ApJ*, 671, 285

Trujillo I., et al. 2006, *ApJ*, 650, 18

Trujillo I., Conselice C. J., Bundy K., Cooper M. C., Eisenhardt P., Ellis R. S. 2007, *MNRAS*, 382, 109

Trujillo I., Cenarro A. J., de Lorenzo-Cáceres A., Vazdekis A., de la Rosa I. G., Cava A., *ApJ*, 692, L118

Trujillo I., Ferreras I., de la Rosa I. G., 2011, *MNRAS*, 415, 3903

Valentinuzzi T. et al. 2010, *ApJ*, 712, 1232

van der Wel A., Bell E. F., van den Bosch F. C., Gallazzi A, Rix H.-W., 2009, *ApJ*, 698, 1232

van der Wel A., Holden B. P., Zirm A. W., Franx M., Rettura A., Illingworth G. D., Ford H. C., 2008, *ApJ*, 688, 48

van der Wel A., et al., 2011, *ApJ*, 730, 38

van de Sande J., et al. 2011, *ApJ*, 736, L9

van Dokkum P. G., et al., 2008, *ApJ*, 677, L5

van Dokkum P. G., Kriek M., Franx M., 2009, *Nat*, 460, 717

van Dokkum P. G., et al., 2010, *ApJ*, 709, 1018

Williams R. E., et al. 1996, *AJ*, 112, 1335

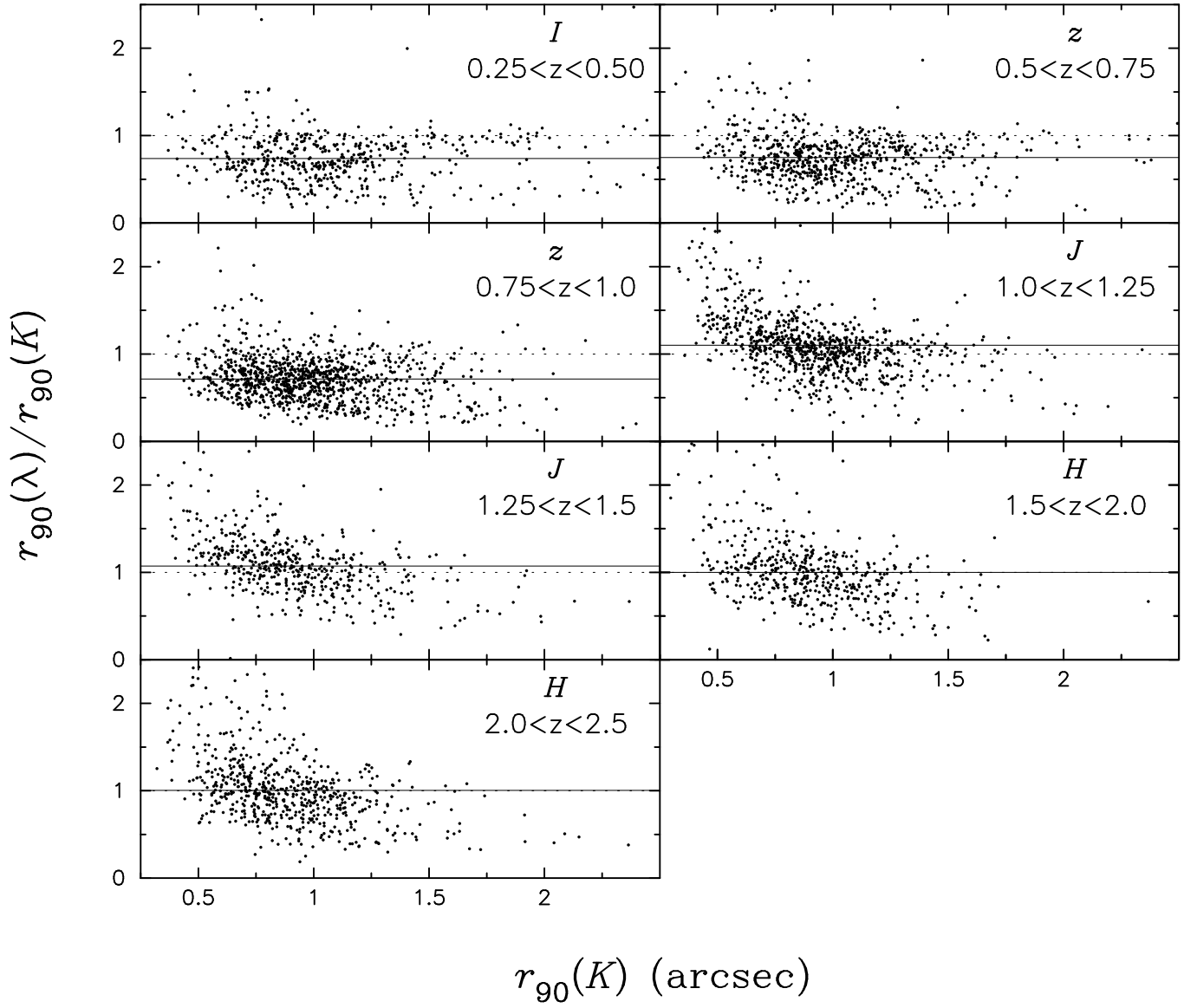


Figure 11. Ratio of 90 percent-light radius (r_{90}^λ) at the nearest rest-frame V band to that of K band (r_{90}^K). Solid line represents the average for the samples in each redshift bin and dotted line is the equal value. The nearest band is depicted at the upper corner for each redshift bin. For I and z bands, we use the HST images binned to $0.117 \text{ arcsec pixel}^{-1}$.

Williams R. J., Quadri R. F., Franx M., van Dokkum P., Toft S.,
 Kriek M., Labbé I., 2010, *ApJ*, 713, 738
 Yamada T., et al., 2009, *ApJ*, 699, 1354
 Zirm A. W., et al., 2007, *ApJ*, 656, 66

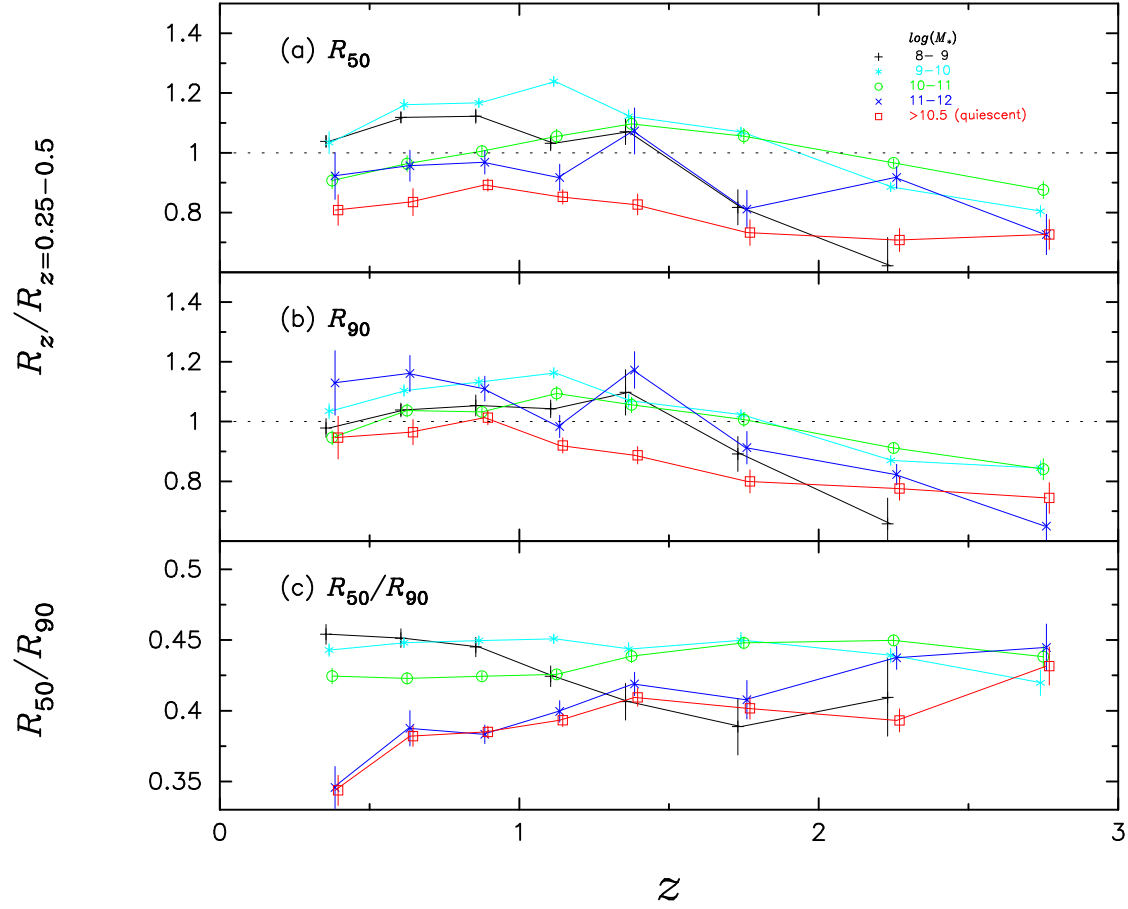


Figure 12. Evolution of galaxy sizes as a function of redshift in stellar mass bins. The ordinate is the difference of the median sizes, (a) R_{50} and (b) R_{90} , from the regression line obtained for the galaxies in $0.25 < z < 0.5$ (Table 2). (c) Median size ratio R_{50}/R_{90} . Unresolved galaxies are included. The error bar is the mean error of the average.